pH-Dependent Conformational Stability of the Ribotoxin α-Sarcin and Four Active Site Charge Substitution Variants †

8 AUTHORS, INCLUDING:

María Flor García-Mayoral
CEPSA
34 PUBLICATIONS   858 CITATIONS

SEE PROFILE

Alvaro Martínez-del-Pozo
Complutense University of Madrid
146 PUBLICATIONS   2,584 CITATIONS

SEE PROFILE

Douglas V Laurents
Spanish National Research Council
73 PUBLICATIONS   1,942 CITATIONS

SEE PROFILE

Marta Bruix
Spanish National Research Council
174 PUBLICATIONS   3,468 CITATIONS

SEE PROFILE

pH-Dependent Conformational Stability of the Ribotoxin α-Sarcin and Four Active Site Charge Substitution Variants[†]

Maria Flor García-Mayoral,[‡] Álvaro Martínez del Pozo,[§] Ramón Campos-Olivas,[‡,||] José G. Gavilanes,[§] Jorge Santoro,[‡] Manuel Rico,[‡] Douglas V. Laurents,[‡] and Marta Bruix*,[‡]

Departamento de Espectroscopía y Estructura Molecular, Instituto de Química-Física Rocasolano, CSIC, Serrano 119, 28006 Madrid, Spain, and Departamento de Bioquímica y Biología Molecular I, Universidad Complutense, Avda. Complutense s/n, 28040 Madrid, Spain

ABSTRACT: α-Sarcin is an exquisitely specific ribonuclease that binds and cleaves a single phosphodiester bond in the large rRNA of the eukaryotic ribosome, inactivating it. To better understand this remarkable activity, the contributions of the active site residues (His 50, Glu 96, and His 137) to the conformational stability have been determined as a function of pH using variant proteins containing uncharged substitutes. Wild-type α-sarcin and the variants are maximally stable near pH 5.5, coinciding with the pH of optimal activity. A comparison of the stability vs pH profiles determined by thermal denaturation experiments to those calculated on the basis of pK_a values shows that the charged forms of Glu 96 and His 137 compromise the enzyme's stability, lowering it. In contrast to barnase, there is little evidence for significant electrostatic interactions in the denatured states of α-sarcin or its active site variants between pH 3.5 and pH 8.5. α-Sarcin contains a long β-hairpin and surface loops which are highly positively charged and which play key roles in membrane translocation and in ribosome binding. These positive charges decrease the stability of α-sarcin, particularly below pH 5. Hydrogen exchange measurements have been performed at pH 5.5 and reveal that the catalytic residues are firmly anchored in highly stable elements of secondary structure. Significant, though lower, levels of protection are observed for many amide protons in the positively charged β-hairpin and long loops.

Refining our comprehension of protein stability is essential for understanding protein structure and function. Stability studies are also important because unstructured and partially unfolded conformations are prone to form aggregates that have been implicated in a large number of human diseases (*1*, *2*). Although hydrogen bonds and hydrophobic interactions make the major contributions to the stability of the folded state of proteins (*3*), they are relatively insensitive to pH. In contrast, the contribution of electrostatic interactions to stability depends on the ionic strength of the solution and the pH, and pH variations can trigger conformational changes which are crucial to protein function. Textbook examples of this important mechanism include the Bohr effect in O_2 binding by hemoglobin and viral membrane fusion proteins (*4*).

The pH dependence of the conformational stability ($\partial \Delta G / \partial$pH) of proteins is linked thermodynamically to the pK_a values of titratable groups in the native (pK_a^N) and denatured (pK_a^D) states (*5*). These pK_a values depend, in turn, on charge−charge, charge−dipole, hydrogen bonds, and desolvation effects in the native and denatured states:

Charge-Charge Charge-Dipole Hydrogen bonds Desolvation

$$\textit{Determine} \quad \downarrow \qquad \uparrow \qquad \textit{Reflect}$$

$$\text{p}K_a^N \quad \text{and} \quad \text{p}K_a^D$$

$$\uparrow\downarrow \quad \textit{Thermodynamically Linked}$$

$$\partial \Delta G / \partial \text{pH}$$

In recent years, it has become clear that, in addition to charge−charge interactions, the presence of hydrogen bonds and the charge−dipole and desolvation effects can induce large shifts (several pH units) in pK_as and consequently can make large (several kilocalories per mole) contributions to $\partial\Delta G/\partial$pH (*6−9*). Moreover, the evidence for the existence of significant electrostatic interactions in unfolded proteins that affect the ensemble distribution of conformations and the pH dependence of stability is increasing (*10−14*). With regard to protein folding, electrostatic interactions have been recently shown to have a remarkably strong effect on the folding kinetics of FynSH3 (*15*).

While the native state pK_a^N values of proteins are generally accessible to study by NMR spectroscopy, and methods are widely available to measure the conformational stability of a protein as a function of pH, the measurement of pK_a^D values

* Corresponding author. Phone: +34915619400 (ext 1455). Fax: +34915642431. E-mail: mbruix@iqfr.csic.es.

[‡] Instituto de Química-Física Rocasolano, CSIC.

[§] Universidad Complutense.

[||] Present address: Centro Nacional de Investigaciones Oncológicas, Melchor Fernández Almagro 3, 28029 Madrid, Spain.

in denatured proteins is technically more difficult. The linkage of pK_a^N, pK_a^D, and $\partial\Delta G/\partial pH$, however, means that pK_a^Ds can be inferred by calculating $\partial\Delta G/\partial pH$ curves with sets of pK_a^D and known pK_a^N values and comparing these curves to those derived from thermal denaturation curves as a function of pH. One objective here is to use this approach to detect electrostatic interactions in the denatured state of the cytotoxic ribonuclease α-sarcin.

Stabilizing interactions allow native proteins to optimally position charged groups at the catalytic site of enzymes. Previous researchers have argued (16−18) that active site charged groups are unlikely to favorably contribute to protein stability, due to the overriding importance of activity. Indeed, buried charged groups of the same sign in close proximity and unfavorable charge−dipole interactions are frequently observed at active sites. These negative contributions to stability are compensated by favorable interactions elsewhere which maintain the enzyme's structural framework. Theoretical (19, 20) and experimental studies (21−23) have generally found that charged groups at the active site destabilize proteins, but a recent study of the RNase Sa has shown that two charged active site groups are stabilizing (24). A distant relative of RNase Sa, α-sarcin, has a much more buried active site. Thus, the second objective of this paper is to determine the contributions of charged groups His 50, Glu 96, and His 137 at the active site of α-sarcin to conformational stability, by studying the $\partial\Delta G/\partial pH$ profiles of variants in which these ionizable groups are conservatively replaced by Gln.

α-Sarcin is an extremely potent cytotoxin that belongs to the fungal ribotoxin family. This enzyme inactivates eukaryotic ribosomes by cleaving a single phosphodiester bond in 28S RNA (25, 26). This enzyme shares a rather low but significant sequence identity with smaller microbial RNases like barnase, RNase Sa, and RNase T1. The latter are noncytotoxic and much less specific. The main factors that determine α-sarcin's cytotoxicity are known to be linked to the structure and high stability of the enzyme, though the relative importance of these factors is still unknown. α-Sarcin is stable over a wide range of pH values (3.5−8.5), and its high-resolution NMR structure (27, 28), dynamic behavior (29), and individual pK_a^N values of residues titrating in this pH range have been determined (30, 31). Compared to smaller noncytotoxic RNases, α-sarcin's structure is characterized by the presence of longer loops for which important roles related to cytotoxicity have been suggested in (i) modulating the ribonuclease activity (N-terminal β-hairpin) (26, 32), (ii) ligand recognition (lysine-rich region of loop 3, N-terminal β-hairpin) (27, 28, 33, 34), and (iii) interaction with biological membranes (loop 2, N-terminal β-hairpin) facilitating the cell entrance by endocytosis (26, 28, 35). The unique orientation of the different loops of the molecule is stabilized by complex networks of interactions different in nature (27), and it is important to determine their stabilities to better understand the biological activities of α-sarcin. Hydrogen exchange monitored by NMR is a very useful technique for determining the conformational stability at the per-residue level. Our third objective here is to use this method to determine the conformational stability of the charged active site residues His 50, Glu 96, and His 137, with peptide groups anchored in the central β-sheet, and of

residues in the long loops which, as mentioned above, play key roles in the cytotoxicity.

In summary, the main goals of the present study are to detect and characterize electrostatic interactions in the denatured state of α-sarcin, to quantify the contributions of the active site residues to the stability and its pH dependence, and to determine the stability at the residue level using NMR monitored hydrogen exchange. These results will provide a better comprehension of α-sarcin's stability and aid the important efforts of theoreticians to develop models for electrostatic interactions in the denatured state and also facilitate the design of new constructs with potential clinical applications such as anticancer agents. These data will also be compared with those from smaller, noncytotoxic microbial RNases, such as RNase T1, Sa, and barnase, which resemble α-sarcin structurally and share the same basic function.

MATERIALS AND METHODS

pH-Dependent Stability Measured by Thermal Denaturation. Folding/unfolding equilibria were followed by CD-monitored thermal denaturation. Circular dichroism spectra were obtained on a Jasco 715 spectropolarimeter at 0.2 nm/s scanning speed; 0.1 and 1.0 cm optical path cells were used in the far- and near-UV, respectively. Mean residue weight ellipticities were expressed in units of deg·cm^2·dmol^{-1}. Thermal denaturation profiles were obtained by measuring the temperature dependence of the ellipticity at 220 nm in the 25−85 °C range; the temperature was changed continuously at a rate of 0.5 °C/min and 0.1 °C increments (36). The protein was dissolved in doubly distilled water deionized with a MilliQ system and containing 50 mM sodium phosphate and 0.1 M sodium chloride. Once the protein was dissolved, the solutions were centrifuged for 10 min at 15000*g*, and the different pH values reported were always directly measured in every single sample studied, using a microelectrode, right before being introduced into the spectrophotometric cuvette. Far-UV CD spectra in the 200−250 nm wavelength range were also taken at the beginning and at the end of each thermal denaturation experiment to assess the conformational state of the samples analyzed at the lowest and highest temperatures employed.

Experimental unfolding free energies were determined assuming a two-state equilibrium between the native and the denatured states, as previously established (37) from DSC measurements. The Gibbs−Helmholtz equation was used to calculate the unfolding free energies with the value of ΔC_p (1.38 kcal mol^{-1} K^{-1}) determined previously (37) for α-sarcin at pH 7.0:

$$\Delta G_{unf} = \Delta H_m\left[1 - \frac{T}{T_m}\right] -$$
$$\Delta C_p\left[(T_m - T) + T\ln\frac{T}{T_m}\right] \quad (1)$$

where T_m is the midpoint transition temperature, ΔH_m is the change in the enthalpy at the temperature T_m, and ΔC_p is the change in the heat capacity during thermal unfolding. Denaturation data were extrapolated to 35 °C, the temperature at which experimental pK_a^N values have been measured (30, 31). Calculations were performed on α-sarcin and four active site mutants, H50Q, E96Q, H137Q, and H50/137Q, assuming

that ΔC_p is temperature independent and unaffected by these mutations.

To obtain the values of T_m and ΔH_m, the CD experimental curves were recorded at different pH values within the range 2.5−8.0 and fit to the equation:

$$\theta(T) = (D_0 + m_D T) - \frac{(D_0 - N_0) + (m_D - m_N)T}{1 + \exp[\Delta H_m(T - T_m)/RTT_m]} \quad (2)$$

where D_0 and N_0 are the extrapolations to 0 K of the temperature-dependent ellipticity variations in the denatured and native states and m_D and m_N represent the slopes of these linear dependences.

pH-Dependent Stability Calculated from pK_a Values in the Native and Denatured States. The dependence of the unfolding free energies ΔG_{D-N} as a function of pH was calculated as described in ref *5*. The folding−unfolding equilibrium constant is determined using the equation:

$$K_{D-N} = K_0 \frac{\prod_{i=1}^{n}(a_{H^+} + K_{a,i}^{D})}{\prod_{i=1}^{n}(a_{H^+} + K_{a,i}^{N})} \quad (3)$$

where K_0 is the folding−unfolding equilibrium constant in the fully protonated protein, a_{H^+} is the proton ion activity which is assumed to be equal to the proton concentration and is calculated from the pH value as 10^{-pH}, and $K_{a,i}^{D}$ and $K_{a,i}^{N}$ are the ionization constants of group i in the denatured and native states, respectively, and can be expressed in terms of the pK_a values as 10^{-pK_a}. The folding−unfolding equilibrium constant in the low pH limit, K_0, has been set equal to 1 since the experimentally measured stability of wild-type α-sarcin is near 0 at low pH. Due to this choice, the curves of the different variants will be in close agreement at very low pH. The equation was evaluated in the pH range from 0 to 10.0 at 0.2 increments. The folding−unfolding constant K_{D-N} is related to the free energy of unfolding by the equation:

$$\Delta G_{D-N} = -RT \ln K_{D-N} \quad (4)$$

Calculations were done for the wild-type protein at 35 °C and compared with those obtained from thermal denaturation experiments. pK_a^N values in the native state were taken from ref *30* (pK_a^N measurements at 35 °C), while pK_a^D values in the denatured state are from Nozaki and Tanford (*38*) corrected to 35 °C. At this point, it should be mentioned that the stability curves depend on the intrinsic pK_a^D values chosen for the unfolded state. Here, the pK_a^D values of Nozaki and Tanford (*38*) have been selected because (i) they are commonly accepted as the consensus values, (ii) they match the pK_a^D values inferred for the denatured states of many proteins (*6, 39, 40*), and (iii) they are very similar to other intrinsic pK_a^D values measured by other authors (*41−45*) in different conditions, particularly for Asp, Glu, and His. However, to ascertain how small changes in the pK_a^D affect ∂ΔG/∂pH, calculations were repeated using the recently reported pK_a^D values of Thulkill et al. (*45*). The Thulkill et

al. values have slightly lower pK_a^D values for Asp (3.67) and Glu (4.25) than those of Nozaki and Tanford (4.0 and 4.4, respectively) and a slightly higher value for His (6.54) than that reported by Nozaki and Tanford (6.3). Only pK_a values of groups titrating in the pH range of the protein stability (3.5−8.5) were considered (Asp, Glu, His, and C-terminus). Electrostatic calculations indicate that Lys, Tyr, and Arg have significantly higher pK_as in the native and denatured states (*31*). Some aspartic acid pK_a^N values (Asp 41, Asp 77, Asp 91, Asp 102, Asp 105) could not be measured in the range of the protein stability, and an upper limit of 3.0 was assigned (*30*). Here a pK_a^N value of 2.6, which best reproduces the experimental ∂ΔG/∂pH results, has been used for calculation purposes.

Calculations for the mutants were performed in a similar fashion, and assuming that pK_a values do not change appreciably, except for titratable groups close to the mutated residues. This assumption is supported by the observation that the mutant protein structures are highly similar to wild-type α-sarcin (*31*). The pK_a^Ns of the active site residues near the mutated site were measured experimentally by NMR for all the mutants, except for His 50 in H137Q, which has a high pK_a^N ($pK_a^N > 8.0$) (*31*). A value of 8.5 was assigned to this group for calculation purposes. A complete list of the pK_a values used, the percent accessible solvent surface area, and the interactions of the ionizable groups used in these calculations are provided in Supporting Information, Tables 1 and 2.

Charge Differences between Native and Denatured States, ΔQ_{D-N}, as a Function of pH. The change in the net charge between the native and denatured protein, which is equivalent to the number of protons taken up during the unfolding acid transition, can be calculated as a function of pH from pK_a values in both states using the Henderson−Hasselbach equation:

$$\Delta Q_{D-N} = \sum_{i=1}^{N}\frac{10^{-\gamma(i)(pH-pK_{a,i}^{D})}}{1 + 10^{-\gamma(i)(pH-pK_{a,i}^{D})}} - \sum_{i=1}^{N}\frac{10^{-\gamma(i)(pH-pK_{a,i}^{N})}}{1 + 10^{-\gamma(i)(pH-pK_{a,i}^{N})}} \quad (5)$$

where $\gamma(i) = -1$ or 1 in the case of an acid or base, respectively. The same pK_a values for the native and denatured states of α-sarcin and the mutants as stated before have been used in these calculations. Because the protonation state of tyrosine, lysine, and arginine residues has been assumed not to change in the range of pH analyzed, these residues do not contribute to the differential net charge in the native and denatured states of α-sarcin and mutants.

Stability Measurements from NMR-Monitored Hydrogen Exchange. Quantitative measurements of NH chemical exchange rates were done from correlation cross-peak intensities observed in a set of HSQC experiments recorded at different times on a solution of [^{15}N]-α-sarcin (concentration 2 mM) in D_2O at pH* 5.2 and 35 °C. pH* is the pH meter reading in D_2O uncorrected for solvent isotope effects. The experimental conditions were selected to ensure that exchange occurs through the EXII exchange mechanism while maintaining the protein at the pH of maximum activity and stability. Due to its very high stability, the complete

exchange of α-sarcin amide protons would occur after a very long period of time. For this reason, we followed the exchange long enough to be able to define the most stable regions of the protein and to obtain information on the stability of the active site and loop regions. Following a dead time (≈30 min), 142 HSQC spectra were recorded consecutively over 308 h. Spectra were processed with the Xwin-NMR package, and correlation cross-peaks were integrated with the UXNMR facility implemented in this program to determine the intensities. A single exponential decay function was fit to the data to obtain the observed exchange rate, k_{obs}. A table containing the exchange rate constants of all measurable NH amide groups is provided in Supporting Information, Table 3. The intrinsic exchange rates for fully denatured α-sarcin, k_{rc}, were calculated using the parameters reported in ref *46* at 35 °C, pH* 5.2. The conformational stability at each amide group was calculated from the ratio of the observed and intrinsic exchange rates:

$$\Delta G_{HX} = -RT \ln(k_{obs}/k_{rc}) =$$
$$-RT \ln K_{op} = -RT \ln(1/P) \quad (6)$$

where K_{op} is the local or global equilibrium constant and P is the protection factor. This treatment assumes that exchange occurs via the EXII mechanism; this assumption typically holds for stable proteins below pH 7.

RESULTS

The pH-dependent stability curves presented in this study have been experimentally measured by thermal denaturation and calculated using the electrostatic model described by Tanford (*5*), assuming pK_a values of model compounds for the denatured state of the proteins.

pH Stability Profiles from Thermal Denaturation Experiments. Figure 1 shows some examples of the thermal denaturation curves of α-sarcin and the different active site mutants near pH 7.0. These data show that relative to wild-type α-sarcin at pH 7.0 (ΔG, 7.0 ± 0.5 kcal/mol), the E96Q variant is more stable (ΔG, 7.7 ± 0.6 kcal/mol), the H50Q and H137Q variants have similar stabilities (ΔG, 6.6 ± 0.5 and 6.2 ± 0.5 kcal/mol, respectively), and the H50/137Q variant is significantly destabilized (ΔG, 4.2 ± 0.3 kcal/mol). Additional thermal denaturation experiments were carried out at various pH values to obtain the data shown in Figure 2. Overall, α-sarcin and its variants show bell-shaped dependences of stability on pH. Though important residues for the catalytic activity are mutated, the $\partial\Delta G/\partial pH$ profiles are not severely altered since these changes at the active site do not disrupt the overall structure.

Wild-type α-sarcin has a maximum stability of 9.8 ± 0.7 kcal/mol near pH 5.5, and the stability decreases markedly as the pH is raised or lowered. The H50Q variant shows a similar profile, with a maximal stability of 9.1 ± 0.7 kcal/mol near pH 5.5. The peak stability of the E96Q mutant (9.8 ± 0.7 kcal/mol) is also reached near pH 5.5, but compared to wild-type α-sarcin, this variant has a higher stability above pH 6, where the Glu carboxylate group is negatively charged (up triangles in Figure 3, left). Interestingly, the H137Q variant, with a maximum stability near pH 5.5 (9.2 ± 0.7 kcal/mol) similar to H50Q, is more stable than wild-type α-sarcin at acidic pH (down triangles in Figure 3, left), where

the imidazole side chain carries a positive charge. These stability differences likely reflect the lower cost of burying the polar side chain of Gln relative to the charged side chains of Glu or His and the higher desolvation penalty (Born energy) for charged Glu and His versus neutral Gln.

The variant carrying the double mutation, H50/137Q, is significantly less stable than wild-type α-sarcin and the other variants at pH 5.5 (6.5 ± 0.5 kcal/mol), although the difference in stability is smaller below pH 4 and above pH 8. Previous NMR studies (*31*) detected significant structural changes in the H50/137Q variant, including the loss of a hydrogen bond between His 137 and Gly 143, and the present results indicate that the two Gln residues at the active site cannot reproduce all of the stabilizing interactions formed by His 50 and His 137.

pH Stability Profiles Calculated from pK_a Values. When $\partial\Delta G/\partial pH$ is calculated using the experimentally determined pK_a^N values and Nozaki and Tanford pK_a^D values, the bell-shaped profiles observed by thermal denaturation are in general successfully reproduced (Figure 2) and the pH values of maximum stability are close for the native protein and the different mutants studied (Figure 3, right). Interestingly, these stability curves also show the higher stability of the E96Q variant at pH values where the wild-type residue Glu 96 is charged. The substantial drop in stability of the H50/137Q double mutant observed by thermal denaturation experiments is not detected by pK_a-based stability calculations.

The reasonably good agreement between the $\partial\Delta G/\partial pH$ profiles determined by thermal denaturation and calculated from the pK_a values constitutes evidence that the Nozaki–Tanford pK_a^D values closely resemble the actual pK_a^D values in denatured α-sarcin and thereby suggests that electrostatic interactions in the denatured state are weak or negligible. However, this agreement is poorer when an alternative set of pK_a^D values are used (Supporting Information, Figure 1). The difference indicates that the calculations are very sensitive to the set of pK_a^D values used. Even very minor changes in the pK_a^D values (i.e., 0.1 pH unit) produce significant alterations in the $\partial\Delta G/\partial pH$ profiles.

Global Protein Charge as a Function of pH. When the pH changes, the net charge and the charge distribution of the protein are altered. Figure 4 (bottom) shows the variation in the net charge between the native and the denatured states of wild-type α-sarcin and the different mutants studied along the pH range. The variation, which is related to the number of protons taken up or released during the unfolding transition, is nearly zero at high and low pH values, where the protein is completely nonprotonated and fully protonated, respectively. Changes are sharper near pH 3.5, ~−4 charge unit change, where the carboxylates titrate. The titration of His residues produces a second region of rather sharp change around pH 7.0, ~2.0−3.0 charge unit change, which is somewhat broader than the carboxylate-induced transition and shows significant variation among the different variants. The first minimum around pH 3.5 (Figure 4, bottom) indicates that the degree of protonation is greater in the denatured states compared to the native states. The opposite holds for the maximum around pH 7.0. All of the curves cross the axis $\Delta Q_{D-N} = 0$ at pH values slightly below 5.0, the pH value of maximum stability calculated on the basis of pK_a values with Tanford's model, so that the proteins are
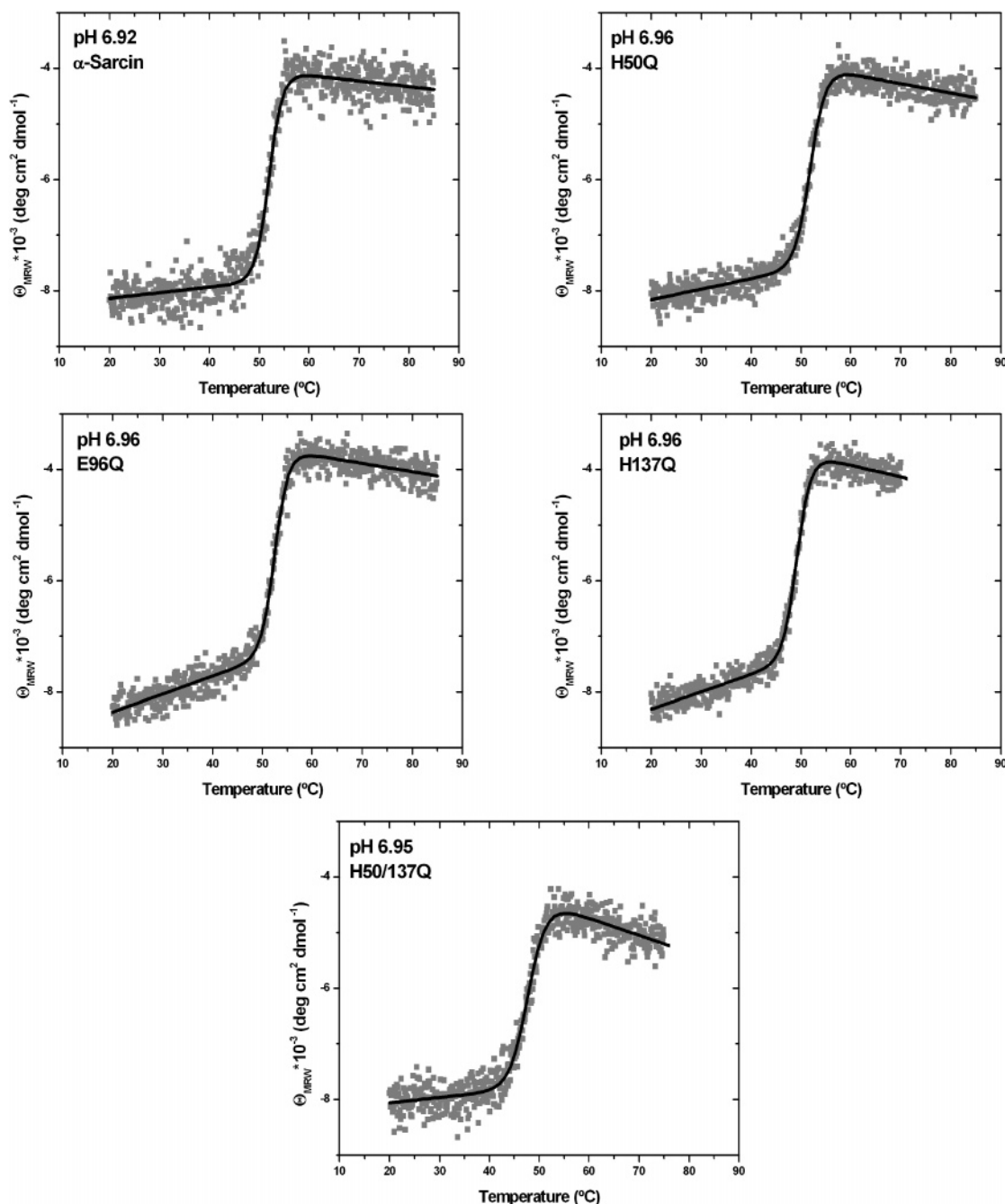
FIGURE 1: Thermal denaturation curves and fitting line for α-sarcin (pH 6.92) and the mutants H50Q (pH 6.96), E96Q (pH 6.96), H137Q (pH 6.96), and H50/137Q (pH 6.95). Θ_{MRW} is the mean residue weight ellipticity measured at 220 nm.

maximally stable at the pH value where the net charges of the native and unfolded conformations are similar.

Calculations of the net charge of the native states of proteins from pK_a^N values also allow the determination of the isoelectric point, p*I*, where the net charge is 0. Calculated p*I* values for the proteins studied are near 10 (Figure 4, top), far away from the pH of maximal stability. Though the number of charged residues is different in the mutants, the p*I* values of native α-sarcin, H50Q, H137Q, and H50/137Q are very close since the His residues are preferentially neutral at this pH, so that the mutation His to Gln does not induce a change in the net charge. The p*I* is slightly higher for the mutant E96Q since the charged form of Glu 96 has been replaced by the polar uncharged Gln side chain. The key observation here is that the pH of maximum stability does

not match the p*I*, indicating the oversimplicity of the model of Linderstrøm-Lang (*47*) which only considers charge−charge interactions and highlighting the important contributions of desolvation, hydrogen bonds, and charge−dipole interactions to the pH dependence of stability.

Residue-Level Stability of α-Sarcin from H/D Exchange Measurements. H/D exchange rates can be measured by NMR to determine the conformational stability at individual backbone amide groups. We have classified the residues of α-sarcin in different groups according to their exchange velocities (Figure 5 and Supporting Information, Table 3). Because of the remarkably high stability of α-sarcin, the exchange of some amide protons is too slow to be measured at the conditions used (pH* 5.2, 35 °C), and only an upper limit for their exchange rate could be estimated. Other surface
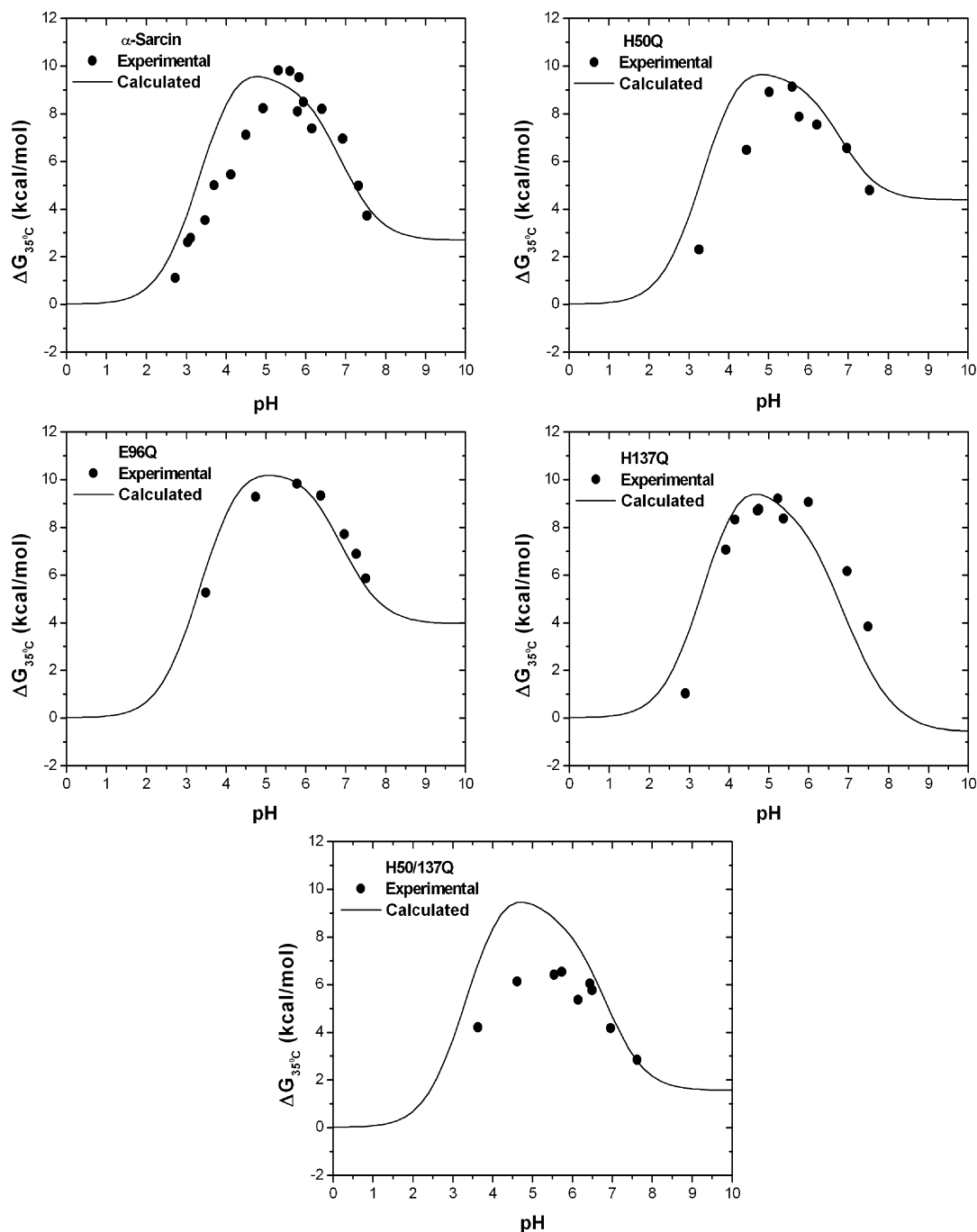
FIGURE 2:   Experimental (black dots) and calculated (curve) pH-dependent stability of α-sarcin and H50Q, E96Q, H137Q, and H50/137Q variants at 35 °C. Estimated average ΔG errors are 7−8% of the actual values (Supporting Information, Table 4).

protons exchange very quickly; a lower limit is given for their exchange rates. The conditions used for the experiment allowed the measurement of exchange rates, k_{obs}, in the range $5.7 \times 10^{-6} < k_{obs} < 4.0 \times 10^{-2}$, and for these protons the free energies of exchange, ΔG_{HX}, were calculated (Figure 5) and found to range from 4 to 9 kcal/mol. Protons belonging to the slowest exchanging group exchange at rates below 5.7×10^{-6} min^{-1}; for this reason, the corresponding free energies of exchange are lower limits and are represented with vertical arrows. The central β-sheet contains most of the slow-exchanging amide groups, though some loop amides also show low exchange rates (Figure 5). Curiously, residues 144 and 145 in β-strand 7 show little protection against exchange and are highly dynamic as detected by NMR

relaxation (*29*). Amide protons on the solvent-exposed face of the helix exchange faster than those in more buried locations. In the N-terminal β-hairpin, the exchange rates generally decrease, moving away from the tight turn at the end of the hairpin toward the protein core. Whereas most NHs in the long loops exchange rapidly, there are also some which exchange slowly. For example, in loop 4 the backbone of Val 130 is completely buried and its NH group belongs to the slowest exchanging class.

Remarkably, the results show that the three active site charged residues, His 50, Glu 96, and His 137, are all firmly anchored in highly stable regions of the backbone (Figure 5). The regions of the backbone corresponding to these residues were also found to be relatively rigid by the NMR
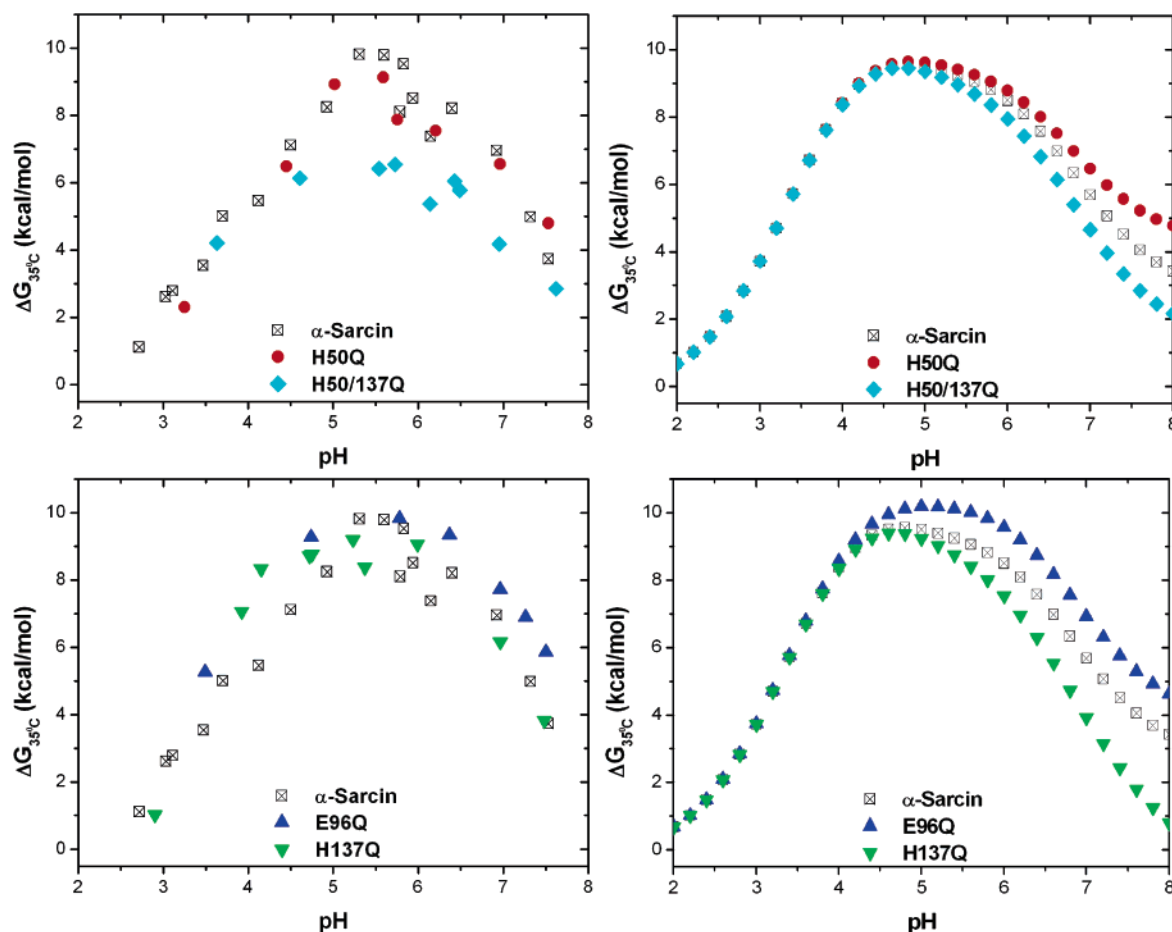
FIGURE 3: Superposition of experimental (left) and theoretically predicted (right) from NMR measured pK_a^N values and Tanford's model pH-dependent stability curves of α-sarcin (crossed squares) and the active site mutants H50Q (red dots), E96Q (blue up triangles), H137Q (green down triangles), and H50/137Q (cyan diamonds) at 35 °C.

dynamic study (*29*). The N-terminal β-hairpin, which is thought to play an active role in membrane translocation and in the interaction with the ribosome, is also surprisingly stable, given its relative independence from the rest of the structure. Its stability ranges from 8 kcal/mol near the base to 5 kcal/mol at the hairpin region farthest away from the protein core.

DISCUSSION

α-Sarcin is the best characterized member of the fungal ribotoxins, a highly specific ribonuclease family. Ribotoxins promote apoptosis of human tumor cells after internalization via endocytosis. On the basis of this activity, ribotoxins, as many other ribonucleases, possess therapeutic promise as anticancer agents (*48, 49*). In the past decade, large efforts have been made to elucidate the different factors that promote ribonuclease cytotoxicity (for a review see ref *50*). Apart from the catalytic activity, it has been shown that the electrostatic properties, mainly the positive net charge, and the protein stability are essential. Furthermore, for a very exquisite enzyme such as α-sarcin it is important that all of these properties are present under the appropriate physiological conditions. In this respect, we have shown that α-sarcin is positively charged below pH 9. This positive charge probably drives the interaction with negatively charged glycolipids and glycoproteins on the outer part of the plasma membrane and promotes the protein internalization as has been proposed for other cytotoxins (*51*).

The extent of interactions between an ionizable residue and the rest of the protein in its native or non-native forms determines its titration properties. Thus, the pK_a value of a particular residue reflects a variety of electrostatic terms arising from different interactions such as charge–charge interactions between the residue and other ionized residues, hydrogen bonds, charge–dipole interactions between the residue and the permanent and induced dipoles of the protein (peptide bonds, polar residues, bound water, helix macrodipoles), the effect of the surrounding solvent, and the desolvation penalty when a charge is removed from solution and placed inside the protein. Consequently, pK_a^Ns of ionizable residues in native proteins are usually distributed over a wide range of values, while pK_a^Ds for the denatured state frequently approach those of model compounds in water. However, although there is not much knowledge about the properties of denatured conformations, there is now confirmed evidence that electrostatic interactions can persist upon denaturation, slightly shifting pK_a^D values, and that the nature of the unfolded state can vary depending on the denaturation process (*52*). In general, strong chemical denaturants like urea or guanidine hydrochloride lead to less compact and more disordered and expanded conformations with residues isolated from molecular interactions than thermal, acid, or pressure-induced denaturation (*5, 53*). In barnase, the acid and thermal denaturation at different ionic strengths was investigated, concluding that these denatured states are sufficiently compact and retain a significant amount
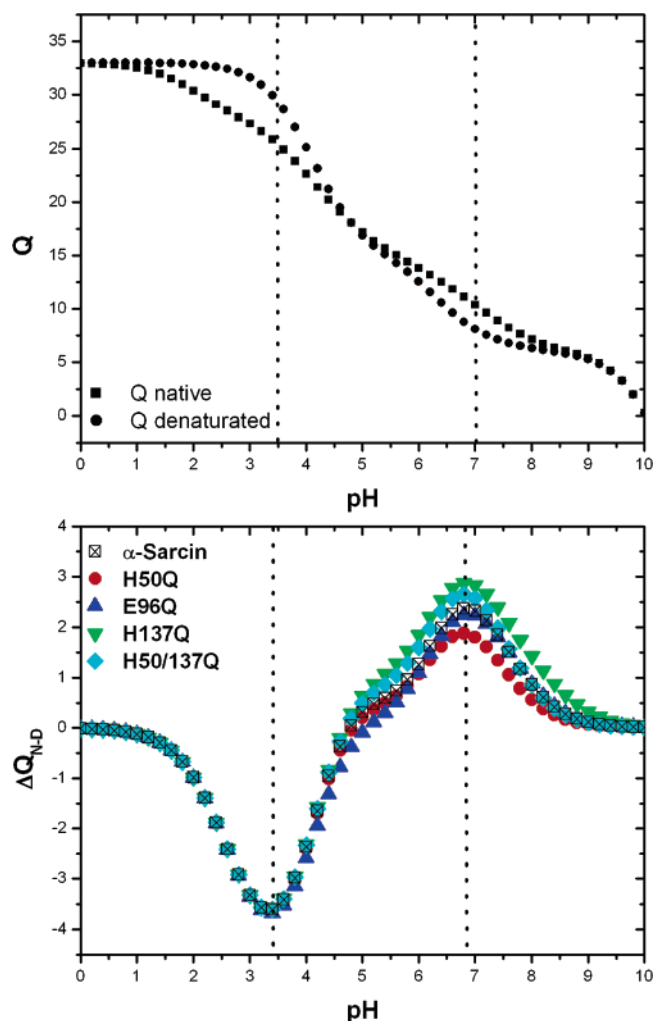
FIGURE 4: (Top) Variation of the α-sarcin total charge in the native (black squares) and denatured (black dots) states as a function of pH. (Bottom) Variation of the charge difference between the native and denatured states of α-sarcin (crossed squares) and the active site mutants H50Q (red dots), E96Q (blue up triangles), H137Q (green down triangles), and H50/137Q (cyan diamonds) as a function of pH at 35 °C.

of residual structure to contain intramolecular charge−charge interactions (*54*). Similar results were obtained for the ovomucoid third domain (*55*) and the barley chymotrypsin inhibitor 2 (*56*), where hydrogen bonds were also found to play an important role in the protein stability. In these cases, an average decrease of 0.3−0.4 pK_a unit for carboxylates in the denatured conformations improved agreement with experiments.

In this paper, α-sarcin pH-dependent stability curves are calculated from the thermodynamic linkage equation described by Tanford that employs the pK_a^N and pK_a^D values of α-sarcin and four active site mutants. This equation contains two implicit assumptions: namely, that (i) there is a two-state equilibrium between the native and the denatured states and (ii) the titration of each group is independent from the others, and no cooperativity occurs. This equation gives only the dependence of ΔG on pH and does not provide absolute values for ΔG. This means that the equation may show a ΔG increase of 5 kcal/mol between pH 2 and pH 7, but whether ΔG is 0 and 5 kcal/mol, respectively, at these pH values, or 5 and 10 kcal/mol remains undefined. Moreover, the success of the equation is highly dependent

on the accuracy and precision of the pK_a values.

Notwithstanding these implicit assumptions and caveats, we have found that this equation reproduces the experimental pH-dependent thermal stability profiles reasonably well when the experimentally determined pK_a^N values for the native conformation and the pK_a^D values of Nozaki and Tanford for the denatured states of α-sarcin and its mutants are used.

pH Dependence of α-Sarcin's Conformational Stability by Thermal Denaturation. The results of the thermal denaturation of wild-type α-sarcin at different pH values show that the protein is highly stable, reaching a maximum of about 10 kcal/mol at pH 5.5, which is also the pH of maximal activity. Although this stability drops off sharply as the pH is raised or lowered, the protein remains stable over a relatively wide pH range (from 3 to 8.5). Possessing a high stability over a wide pH range is probably important physiologically, since α-sarcin must diffuse first through an environment between fungi which is often acidic and then through the mildly alkaline cytoplasm of the target hypha.

Is α-Sarcin's Stability Compromised by Activity? In general, a fair portion of the conformational stability of a protein is thought to be "spent" to maintain active site groups in orientations that are optimal for geometry. However, a recent, stimulating paper by Pace and co-workers has shown that, in the case of RNase Sa, one catalytic residue, Glu 54, is stabilizing relative to Gln, whereas the substitution of the second catalytic residue, His 85, by Gln has no significant effect on the stability. In this paper, we have used site-directed mutagenesis to study the contribution of the active site residues, His 50, Glu 96, and His 137, to the conformational stability of α-sarcin as a function of pH. The results show that both catalytic residues, Glu 96 and His 137, destabilize the native state of α-sarcin when they are charged, though this destabilization is rather mild. Although RNase Sa and α-sarcin are distantly related, this difference could be related to the fact that the catalytic groups are more buried in the case of α-sarcin; the percent solvent-accessible surface of His 50, Glu 96, and His 137 is only 18%, 1%, and 46%, respectively (*27*, *31*), compared to 10% and 45% for Glu 54 and His 85, respectively, in RNase Sa (*57*). The desolvation cost of burying a charge in an environment where it cannot form compensating interactions is quite large, costing several kilocalories per mole of free energy (*8*, *58*). The lack of severe destabilizing contributions of the charged forms of His 50, Glu 96, and His 137, reported here, provides further evidence in favor of the existence of a highly optimized network of electrostatic interactions at the active site which compensates for the desolvation cost. The existence of this network of interactions was previously proposed on the basis of a study of the experimentally determined and theoretically calculated pK_a^N values (*31*).

Besides the charged groups at the active site, α-sarcin contains a large number of positively charged groups in the N-terminal β-hairpin and the long loops which have been reported to play key roles in the translocation of the protein across membranes (*59*), as well as in the initial binding to the ribosome and the rapid 2D diffusion across its surface to reach the cleavage site (*60−62*). On the basis of the model of Linderstrøm-Lang (*47*) it is expected that the unfavorable charge−charge interactions produced by this high density of positive charges (α-sarcin contains 20 Lys, 4 Arg, 6 His, and only 11 Asp and 6 Glu) will destabilize the folded
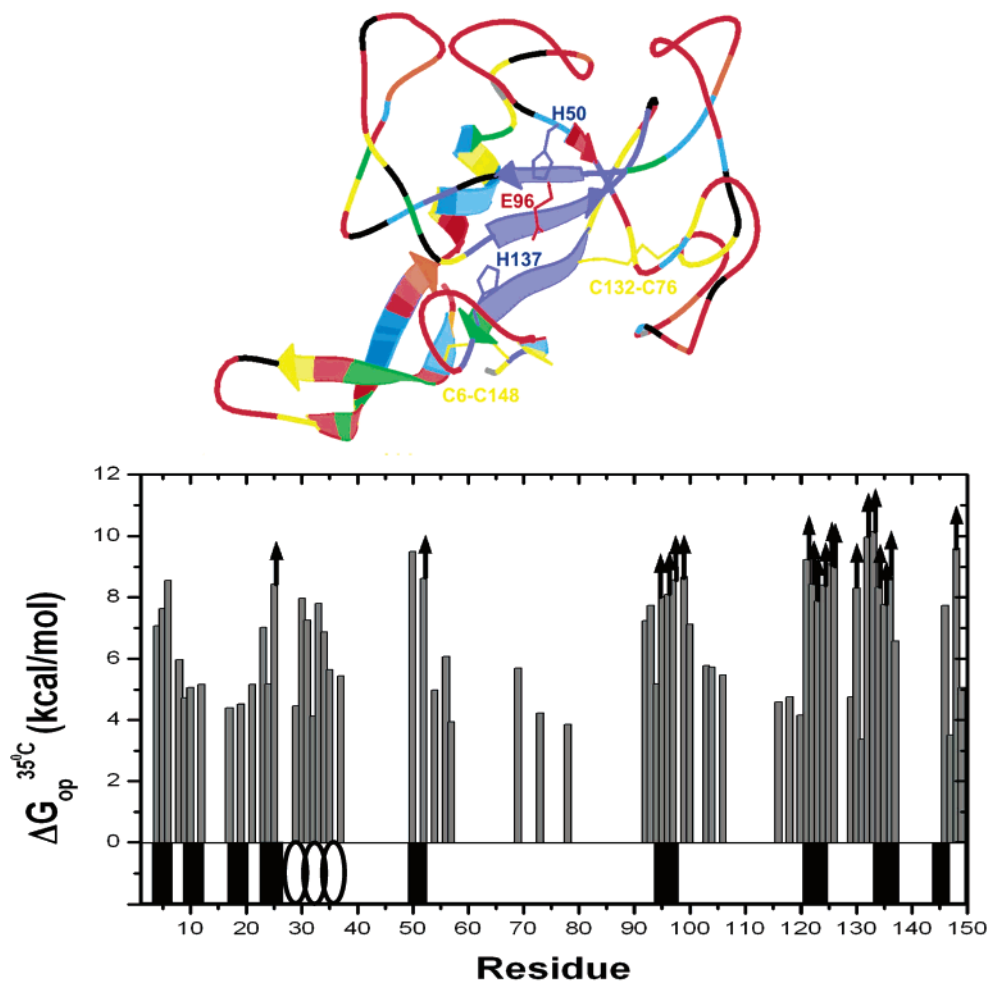
FIGURE 5: (Top) Ribbon diagram of α-sarcin, with residues colored according to the exchange rates (in min^{-1}) at pH* 5.2, 35 °C, of their NH groups: red, $k_{ex} > 0.094$; orange, $0.094 < k_{ex} < 0.04$; yellow, $0.04 < k_{ex} < 0.01$; green, $0.01 < k_{ex} < 0.001$; sky blue, $0.001 < k_{ex} < 5.7 \times 10^{-6}$; blue, $k_{ex} < 5.7 \times 10^{-6}$. No satisfactory fits could be obtained for the amide groups of His 36, Phe 71, and His 150 (shaded gray). Proline residues are shown in black and the two disulfide bonds linking Cys 6−Cys 148 and Cys 76−Cys 132 in orange. (Bottom) α-Sarcin's per residue stability at pH* 5.2 and 35 °C obtained from amide $^{1}H/^{2}H$ exchange rates. Higher energy values than those shown with gray columns are indicated by black arrows. Secondary structure is indicated: β-strands as rectangles and α-helix as circles. The first four strands are integrated in the N-term β-hairpin, followed by the α-helix and strands β3−β7. Inserted between the helix and each strand are loops 1−5.

α-sarcin, particularly as the pH is lowered and the negatively charged carboxylate groups are neutralized. Therefore, we can propose that part of the α-sarcin's conformational stability is sacrificed for the essential activities performed by the positively charged surface groups.

Are There Electrostatic Interactions in the Denatured State of α-Sarcin? The reasonably good agreement observed here for the experimentally determined ∂ΔG/∂pH profiles and those calculated on the basis of the native state pK_a^Ns and the intrinsic pK_a^Ds reported by Nozaki and Tanford indicates that the pK_a^D values in the denatured state of α-sarcin are not strongly altered. This is an interesting and important result considering that for other ribonucleases with an excess of positive charges, such as barnase (*10*) or bovine pancreatic RNase A (*63*, *64*), lowered carboxylate group pK_a^D values need to be invoked for the denatured state (and, therefore, significant electrostatic interactions are present in the unfolded state) to achieve ∂ΔG/∂pH profiles that are in reasonably good agreement with the experimentally determined ∂ΔG/∂pH profiles. This suggests that the unfolding of α-sarcin might be especially thorough. However, considering that some variation has been observed in the pK_a^D

values reported by different laboratories (±0.3 to ±0.5 pH unit) (*45*, *65*), the presence of some electrostatic interactions in denatured α-sarcin cannot be completely ruled out.

Thermal- and pK$_a$-Based Calculated Stabilities of α-Sarcin and H50Q, E96Q, H137Q, and H50/137Q Mutants as a Function of pH. The thermodynamic equation linking stability and pK_as gives well-reproduced pH-dependent stability profiles for the proteins studied, although a slight shift in the maximum (0.5 pH unit) is observed in all cases. The pH of maximum stability is 5.5, close to the pH of maximal function in vitro measured against dinucleotides (*30*) and far away from the isoelectric point of the folded protein (p*I* ≈ 10). This is not surprising as a recent analysis which includes an important number of enzymes has shown that there is no correlation between the isoelectric point and the pH of optimal stability (*66*). Thus, α-sarcin joins the list of enzymes including the remotely related RNase Sa (*67*) which are most stable when they carry net charge. Additionally, the net charge of native α-sarcin at the pH of maximum stability is positive, a tendency observed in other proteins with acidic optimal pH (*66*).

The conservation of the characteristic profile of the stability curves in native α-sarcin and the mutants is a clear proof that local conformational changes take place in the vicinity of the mutated residues without disturbing the global fold. This result supports the NMR evidence that most ionizable residues maintain pK_a^N values similar to those of wild-type α-sarcin and that the factors that stabilize the native conformation are maintained.

It is interesting that the pH stability profile and the in vitro activity curves are in close agreement (*30*). It is well-known that these curves can overlap totally (as in this case), partially, or be largely shifted one with respect to the other. In this regard, α-sarcin could be a good model to learn about the stabilization forces that make possible this agreement. This information could be useful in basic and applied fields as, for example, in the design of more efficient industrial enzymes.

Role of Salt Bridges in α-Sarcin's Stability. The linkage equation reported by Tanford allows the ionizable residues of α-sarcin to be rapidly classified depending on their favorable or unfavorable contribution to stability. The lower the pK_a value of a residue in the native state compared to the denatured state, the more the conjugate base stabilizes the folded structure with respect to the unfolded structure, and vice versa. This contribution is enhanced in the range of pH values where amino acids titrate.

The most perturbed pK_a^N values in α-sarcin are those of Asp 41, Asp 77, Asp 91, Asp 102, and Asp 105. All have lowered pK_a^N values (by 1.4 pH unit on average), and all except for Asp 91 form salt bridges. Of these, the Asp 41−His 82 salt bridge is essentially buried whereas the others are near the protein surface. Many studies addressed to evaluate the contribution of salt bridges to protein stability have shown that those highly exposed to the solvent generally make little contribution to protein stability due to the higher value of the dielectric constant near the surface (*68*) and the entropic cost of fixing mobile side chains in the optimum conformation for the establishment of electrostatic interactions. However, the Coulombic interactions between surface charges can be optimized to achieve important increases in conformational stability (*69, 70*), and this appears to be an evolutionary strategy for the stabilization of thermophilic proteins (*71, 72*). Applying such a strategy to improve the conformational stability of α-sarcin would be complicated because of the important physiological roles of the surface charges.

The pK_a difference ($pK_a^N - pK_a^D$) for His 82 is also important (1 pH unit), making the contribution of the Asp 41−His 82 salt bridge to α-sarcin's stability always favorable in the whole pH range, and particularly at those pH values (between 4 and 6.5) where the carboxylic group is deprotonated and the imidazole ring is still protonated (Figure 6). The larger pK_a shift of Asp 41 compared to His 82 is due to an additional hydrogen bond formed between Asp 41 and Trp 51 (*27*), which highlights the role of hydrogen bonds in shifting pK_a values as emphasized by Robertson and co-workers (*9, 73*). In this pH range, the contribution of the salt bridge varies from 1.5 to 1.9 kcal/mol. The conservation of both residues in most members of the *Aspergillus* ribotoxin family speaks to the importance of this salt bridge in the stability of α-sarcin.
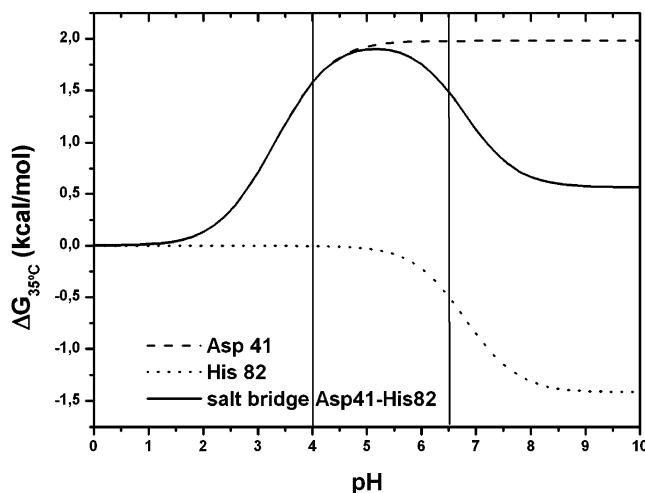

FIGURE 6: Contribution of the Asp 41−His 82 salt bridge to the conformational stability of α-sarcin according to Tanford's electrostatic model.

Relationships between H/D Exchange and Molecular Structure. Hydrogen exchange measurements provide data on the stability at individual amide groups. In α-sarcin, a group of residues with high protected factors against exchange could be identified: Cys 6, Tyr 25, His 50, Phe 52, Leu 95, Glu 96, Phe 97, Thr 99, Arg 121−Tyr 126, Val 130, Cys 132−Ala 136, and Cys 148. Most of these residues belong to the central β-sheet, form hydrogen bonds with carboxyl oxygens from consecutive β-strands, and are deeply buried in the hydrophobic core of the protein. Some of these residues belong to the two major hydrophobic clusters of α-sarcin, the larger one made up by the disulfide bridge Cys 76−Cys 132. All of these residues must exchange essentially by global unfolding and define the most rigid and stable part of the molecule (strands $\beta_3-\beta_6$ and internal N-terminal β-sheet). Local fluctuations are the main mechanism of exchange for a large number of protons belonging to loops 1, 2, 3, and 5, the C-terminal strand β_7, and the most solvent-exposed part of the N-terminal β-hairpin. Nonetheless, many amide groups in the loops and N-terminal β-hairpin show significantly slowed exchange rates. Considering that NMR relaxation studies have shown that these are the most dynamic regions of α-sarcin (*29*), their significant protection to hydrogen exchange suggests that these regions move and flex in a concerted way that generally maintains the local network of hydrogen bonds. The first part of the α-helix (Gln 27, Asn 28) is also highly mobile and shows low protection against hydrogen exchange. In the N-terminal β-hairpin, the decrease observed in k_{obs} moving away from the turn presents an interesting contrast to the corresponding increase observed in model β-hairpins (*74*). This difference is surely due to the fact that, in α-sarcin, the ends of this β-hairpin are connected to the rest of the protein, whereas the ends of β-hairpin peptides are free to fray. The high stability of this part of the protein is likely to be important as it is essential for the ribotoxin-specific recognition of the ribosome.

Individual Contributions of Active Site Residues to α-Sarcin's Stability from Electrostatic Approaches. Factors Contributing to the Stabilization in α-Sarcin Mutants. The role of catalytic residues in protein stability has been controversial and has not been fully elucidated yet. Several authors
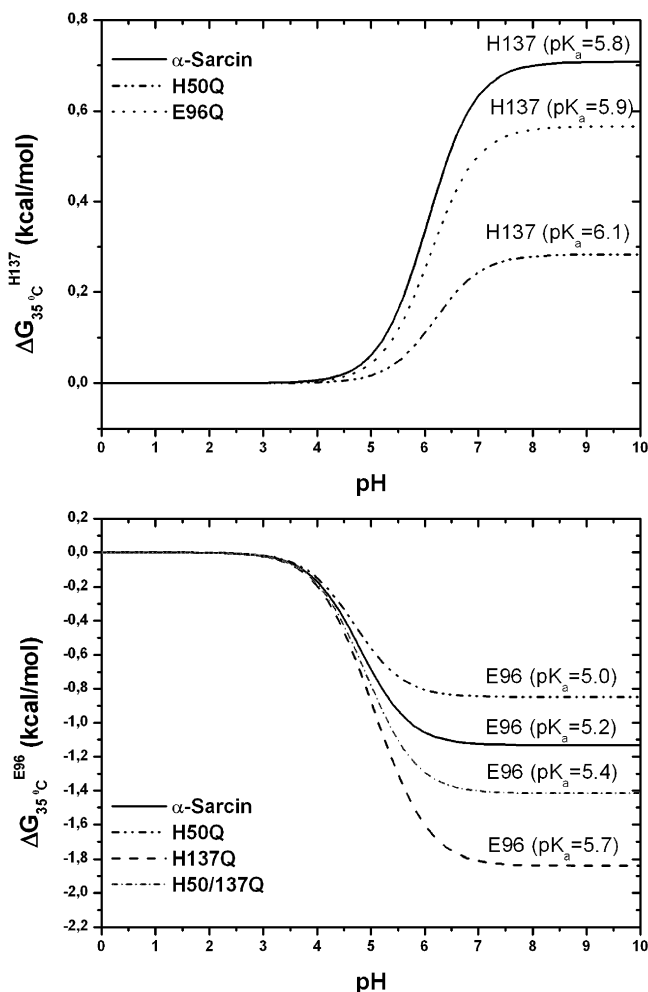
FIGURE 7: Comparison of individual contributions of the catalytic residues (Glu 96, His 137) of α-sarcin and H50Q, E96Q, H137Q, and H50/137Q variants to global stability according to Tanford's electrostatic model.

reported that active site residues were optimized for catalysis but not for stability, and their contribution can be largely destabilizing as proved experimentally (*21, 22*) and theoretically (*19, 20*). This is consistent with the presence of some flexibility at the active sites to properly carry out the biological function (*75, 76*). However, there is an interesting example of catalytic residues contributing favorably to protein stability as well (*24*).

Previous studies on α-sarcin have shown that a perfect balance and equilibrium of electrostatic interactions in the active site is necessary for the optimal activity of the ribotoxin (*31*) and that the specific pK_a^N values of the catalytic couple are crucial for the functioning of His 137 as an acid and Glu 96 as a base in the transphosphorylation step of the cyclizing mechanism (*30*). The electrostatic calculations show that the charged forms of Glu 96 and His 137 (Figure 7) make destabilizing contributions of 1.1 and 0.7 kcal/mol, respectively, in wild-type α-sarcin. A similar pattern of behavior is observed for α-sarcin mutants holding these side chain groups. As mentioned, the mutant E96Q is the most stable above pH 5.5 because the unfavorable contribution of Glu 96 is lost, and that of the uncharged His 50 (pK_a^N 6.4) almost disappears. The mutant H137Q is more stable below pH 5.5, because the unfavorable contribution of the charged imidazole group is lost. For H50Q, as the

charged form of His 50 confers additional stability to wild-type α-sarcin, this mutant is slightly less stable at acidic pH where the charged form of the imidazole group is more populated. The electrostatic predictions explain, in general, the experimental data for these mutants. The largest discrepancies occur in the mutant H50/137Q. The pK_a-based electrostatic model is unable to reproduce the remarkable stability loss observed in the range covering the pH of maximum stability. In this case we propose that structural reorganizations affecting the efficiency of the hydrophobic/ packing interactions at the active site induced by the double substitution and the larger entropic cost of fixing the Gln side chains compared to the cyclic aromatic side chains are the more likely pH-independent factors decreasing the stability of this mutant.

Comparison with Other Ribonucleases. The dependence of the conformational stability on pH has also been studied for barnase (*54, 77*), RNase T1, and RNase Sa (*67*), much smaller microbial ribonucleases distantly related to α-sarcin. They lack the long loops of α-sarcin, show much less specificity than α-sarcin but have much higher substrate turnovers, and are noncytotoxic. Barnase (pI = 9.2), like α-sarcin, carries an excess of positively charged residues. However, on the basis of the comparison of its experimentally determined $\partial\Delta G/\partial$pH profile to that calculated using pK_a^N values, Nozaki–Tanford pK_a^D values (*38*), and Tanford's equation, it was concluded that depressed carboxylate pK_a^D values, and therefore significant electrostatic interactions, exist in the denatured state (*10*). This is interesting since the denaturant-induced unfolding of barnase, which lacks disulfide bonds, was reported to be very thorough (*77*).

In contrast to α-sarcin and barnase, RNase T1 (pI = 3.8, two disulfide bonds) and RNase Sa (pI = 3.5, one disulfide bond) carry an excess of negatively charged residues. The good agreement between their experimentally determined $\partial\Delta G/\partial$pH profiles and those calculated from their known pK_a^N (*6, 78, 79*) and Nozaki–Tanford pK_a^D values (*38*) suggests that any electrostatic interactions that may exist in their denatured states are energetically modest or negligible (*80*) (Laurents et al., unpublished observations). Interestingly, the variant of RNase Sa called "5K" (pI = 10.2) that carries five surface carboxylate to lysine substitutions has the same $\partial\Delta G/\partial$pH and activity vs pH dependences as the wild-type enzyme (*67*). However, on the basis of the pK_a^N values of 5K (*79*) and Nozaki–Tanford (*38*) pK_a^D values, significant electrostatic interactions appear to be present in the denatured state of this positively charged RNase Sa variant (*80*) (Laurents et al., unpublished observations). Direct measurements of pK_a^D values in unfolded RNase Sa and 5K to corroborate these intriguing findings are technically challenging but are currently underway. Direct and conclusive evidence for perturbed pK_a^D values has been reported for the small SH3 drk domain (*40*).

One question that needs some attention is to clarify if the different profiles of $\partial\Delta G/\partial$pH can be related with the properties of the different members of the ribonuclease family. As we have shown here, α-sarcin, like RNase T1, RNase Sa, and RNase Sa 5K, shows a defined maximum of stability at acidic pH (*67, 81*). This stability decreases more or less rapidly when moving away from this pH value. However, other ribonucleases, such as RNase A, barnase, and others (*81*), show a broad plateau of stability covering

a wide range of pHs, normally from pH 5 to pH 9. It is well-known that the pH influences not only the stability but also the function of an enzyme and that enzymes operate optimally at a particular pH. These differences could be telling us that the first group of proteins has been designed to work preferentially in more restricted pH conditions than the other ones. In this respect, the physiological pH is not homogeneous and varies in different locations in the cell and the body (*66*). Since α-sarcin is maximally stable and active in mildly acidic conditions such as the interstitial fluid of solid tumors (*66*), it may hold particular promise as an anticancer therapeutic agent.

In conclusion, the results shed new light on the contribution of the charged catalytic and surface residues to the conformational stability of α-sarcin. These results aid in the continuing efforts of many groups to develop anticancer therapeutics based on ribotoxins.

SUPPORTING INFORMATION AVAILABLE

Table 1 with the pK_a values, the percent accessible surface area, and the interactions of the ionizable groups used in the calculations; Table 2 with the experimental pK_a values of H50Q, E96Q, H137Q, and H50/137Q α-sarcin variants used in the calculations; Table 3 showing the $^1H/^2H$ exchange rate constants of α-sarcin amide protons at pH* 5.2 and 35 °C; Table 4 with values of T_m, ΔH_m, and ΔG at 35 °C at each measured pH for α-sarcin and H50Q, E96Q, H137Q, H50/137Q variants; Figure 1 showing a comparison of the $\partial\Delta G/\partial pH$ profiles for α-sarcin calculated with two different sets of pK_a^D values. This material is available free of charge via the Internet at http://pubs.acs.org.

REFERENCES

1. Stefani, M., and Dobson, C. M. (2003) Protein aggregation and aggregate toxicity: new insights into protein folding, misfolding diseases and biological evolution, *J. Mol. Med. 81*, 678−699.

2. Quist, A., Doudevski, I., Lin, H., Azimova, R., Ng, D., Frangione, B., Kagan, B., Ghiso, J., and Lal, R. (2005) Amyloid ion channels: a common structural link for protein-misfolding disease, *Proc. Natl. Acad. Sci. U.S.A. 102*, 10427−10432.

3. Pace, C. N., Shirley, B. A., McNutt, M., and Gajiwala, K. (1996) Forces contributing to the conformation stability of proteins, *FASEB J. 10*, 75−83.

4. Bullough, P. A., Hughson, F. M., Skehel, J. J., and Wiley, D. C. (1994) Structure of influenza haemagglutinin at the pH of membrane fusion, *Nature 371*, 37−43.

5. Tanford, C. (1970) Protein denaturation. C. Theoretical models for the mechanism of denaturation, *Adv. Protein Chem. 24*, 1−95.

6. Giletto, A., and Pace, C. N. (1999) Buried, charged, non-ion-paired aspartic acid 76 contributes favorably to the conformational stability of ribonuclease T1, *Biochemistry 38*, 13379−13384.

7. Laurents, D. V., Scholtz, J. M., Rico, M., Pace, C. N., and Bruix, M. (2005) Ribonuclease Sa conformational stability studied by NMR-monitored hydrogen exchange, *Biochemistry 44*, 7644−7655.

8. Stites, W. E., Gittis, A. G., Lattman, E. E., and Shortle, D. (1991) In a staphylococcal nuclease mutant the side-chain of a lysine replacing valine 66 is fully buried in the hydrophobic core, *J. Mol. Biol. 221*, 7−14.

9. Li, H., Robertson, A. D., and Jensen, J. H. (2005) Very fast empirical prediction and rationalization of protein pK_a values, *Proteins 61*, 704−721.

10. Oliveberg, M., Arcus, V. L., and Fersht, A. R. (1995) pK_a values of carboxyl groups in the native and denatured states of barnase: the pK_a values of denatured state are on average 0.4 units lower than those of model compounds, *Biochemistry 34*, 9424−9433.

11. Pace, C. N., Alston, R. W., and Shaw, K. L. (2000) Charge-charge interactions influence the denatured state ensemble and contribute to protein stability, *Protein Sci. 9*, 1395−1398.

12. Pradeep, L., and Udgaonkar, J. B. (2004) Effect of salt on the urea-unfolded form of barstar probed by m value measurements, *Biochemistry 43*, 11393−11402.

13. Cho, J. H., and Raleigh, D. P. (2006) Electrostatic interactions in the denatured state and in the transition state for protein folding: effects of denatured state interactions on the analysis of transition state structure, *J. Mol. Biol. 359*, 1437−1446.

14. Li, Y., Horng, J. C., and Raleigh, D. P. (2006) pH dependent thermodynamic and amide exchange studies of the C-terminal domain of the ribosomal protein L9: implications for unfolded state structure, *Biochemistry 45*, 8499−8506.

15. de Los Rios, M. A., and Plaxco, K. W. (2005) Apparent Debye-Huckel electrostatic effects in the folding of a simple, single domain protein, *Biochemistry 44*, 1243−1250.

16. Williams, R. J. (1972) The entatic state, *Cold Spring Harbor Symp. Quant. Biol. 36*, 53−62.

17. Richards, F. M. (1974) The interpretation of protein structures: total volume, group volume distributions and packing density, *J. Mol. Biol. 82*, 1−14.

18. Warshel, A. (1978) Energetics of enzyme catalysis, *Proc. Natl. Acad. Sci. U.S.A. 75*, 5250−5254.

19. Warshel, A. (1998) Electrostatic origin of the catalytic power of enzymes and the role of preorganized active sites, *J. Biol. Chem. 273*, 27035−27038.

20. Elcock, A. H. (2001) Prediction of functionally important residues based solely on the computed energetics of protein structure, *J. Mol. Biol. 312*, 885−896.

21. Meiering, E. M., Serrano, L., and Fersht, A. R. (1992) Effect of active site residues in barnase on activity and stability, *J. Mol. Biol. 225*, 585−589.

22. Beadle, B. M., and Shoichet, B. K. (2002) Structural bases of stability-function tradeoffs in enzymes, *J. Mol. Biol. 321*, 285−296.

23. Shoichet, B. K., Baase, W. A., Kuroki, R., and Matthews, B. W. (1995) A relationship between protein stability and protein function, *Proc. Natl. Acad. Sci. U.S.A. 92*, 452−456.

24. Yakovlev, G. I., Mitkevich, V. A., Shaw, K. L., Trevino, S., Newsom, S., Pace, C. N., and Makarov, A. A. (2003) Contribution of active site residues to the activity and thermal stability of ribonuclease Sa, *Protein Sci. 12*, 2367−2373.

25. Endo, Y., and Wool, I. G. (1982) The site of action of alpha-sarcin on eukaryotic ribosomes. The sequence at the alpha-sarcin cleavage site in 28 S ribosomal ribonucleic acid, *J. Biol. Chem. 257*, 9054−9060.

26. García-Ortega, L., Lacadena, J., Mancheño, J. M., Oñaderra, M., Kao, R., Davies, J., Olmo, N., Martínez del Pozo, A., and Gavilanes, J. G. (2001) Involvement of the amino-terminal beta-hairpin of the *Aspergillus* ribotoxins on the interaction with membranes and nonspecific ribonuclease activity, *Protein Sci. 10*, 1658−1668.

27. Pérez-Cañadillas, J. M., Santoro, J., Campos-Olivas, R., Lacadena, J., Martínez del Pozo, A., Gavilanes, J. G., Rico, M., and Bruix, M. (2000) The highly refined solution structure of the cytotoxic ribonuclease alpha-sarcin reveals the structural requirements for substrate recognition and ribonucleolytic activity, *J. Mol. Biol. 299*, 1061−1073.

28. García-Mayoral, M. F., Pantoja-Uceda, D., Santoro, J., Martínez del Pozo, A., Gavilanes, J. G., Rico, M., and Bruix, M. (2005) Refined NMR structure of alpha-sarcin by $^{15}N-^1H$ residual dipolar couplings, *Eur. Biophys. J. 34*, 1057−1065.

29. Pérez-Cañadillas, J. M., Guenneugues, M., Campos-Olivas, R., Santoro, J., Martínez del Pozo, A. M., Gavilanes, J. G., Rico, M., and Bruix, M. (2002) Backbone dynamics of the cytotoxic ribonuclease alpha-sarcin by N-15 NMR relaxation methods, *J. Biomol. NMR 24*, 301−316.

30. Pérez-Cañadillas, J. M., Campos-Olivas, R., Lacadena, J., Martínez del Pozo, A., Gavilanes, J. G., Santoro, J., Rico, M., and Bruix, M. (1998) Characterization of pK_a values and titration shifts in the cytotoxic ribonuclease alpha-sarcin by NMR. Relationship between electrostatic interactions, structure, and catalytic function, *Biochemistry 37*, 15865−15876.

31. García-Mayoral, M. F., Pérez-Cañadillas, J. M., Santoro, J., Ibarra-Molero, B., Sanchez-Ruiz, J. M., Lacadena, J., Martínez del Pozo, A., Gavilanes, J. G., Rico, M., and Bruix, M. (2003) Dissecting structural and electrostatic interactions of charged groups in alpha-sarcin. An NMR study of some mutants involving the catalytic residues, *Biochemistry 42*, 13122−13133.

32. Kao, R., and Davies, J. (1999) Molecular dissection of mitogillin reveals that the fungal ribotoxins are a family of natural genetically engineered ribonucleases, *J. Biol. Chem. 274*, 12576−12582.

33. Hwu, L., Huang, K. C., Chen, D.-T., and Lin, A. (2000) The action mode of the ribosome-inactivating protein alpha-sarcin, *J. Biomed. Sci. 7*, 420−428.

34. García-Ortega, L., Masip, M., Mancheño, J. M., Oñaderra, M., Lizarbe, M. A., García-Mayoral, M. F., Bruix, M., Martínez del Pozo, A., and Gavilanes, J. G. (2002) Deletion of the NH2-terminal beta-hairpin of the ribotoxin alpha-sarcin produces a nontoxic but active ribonuclease, *J. Biol. Chem. 277*, 18632−18639.

35. De Antonio, C., Martínez del Pozo, A., Mancheño, J. M., Oñaderra, M., Lacadena, J., Martínez Ruiz, A., Pérez-Cañadillas, J. M., Bruix, M., and Gavilanes, J. G. (2000) Assignment of the contribution of the tryptophan residues to the spectroscopic and functional properties of the ribotoxin alpha-sarcin, *Proteins 41*, 350−361.

36. Martínez del Pozo, A., Gasset, M., Oñaderra, M., and Gavilanes, J. G. (1988) Conformational study of the antitumor protein alpha-sarcin, *Biochim. Biophys. Acta 953*, 280−288.

37. Gasset, M., Mancheño, J. M., Laynez, J., Lacadena, J., Fernández-Ballester, G., Martínez del Pozo, A., Oñaderra, M., and Gavilanes, J. G. (1995) Thermal unfolding of the cytotoxin alpha-sarcin: phospholipid binding induces destabilization of the protein structure, *Biochim. Biophys. Acta 1252*, 126−134.

38. Nozaki, Y., and Tanford, C. (1967) Examination of titration behavior, *Methods Enzymol. 11*, 715−734.

39. Kay, M. S., and Baldwin, R. L. (1998) Alternative models for describing the acid unfolding of the apomyoglobin folding intermediate, *Biochemistry 37*, 7859−7868.

40. Tollinger, M., Crowhurst, K. A., Kay, L. E., and Forman-Kay, J. D. (2003) Site-specific contributions to the pH dependence of protein stability, *Proc. Natl. Acad. Sci. U.S.A. 100*, 4545−4550.

41. Cohn, E. J., and Edsall, J. T. (1943) *Proteins, Amino Acids and Peptides*, Hafner Publishing Co., New York.

42. Gurd, F. R. N., Keim, P., Glushko, V. G., Lawson, P. J., Marshall, R. C., Nigen, A. M., and Vigna, R. A. (1972) in *Chemistry and Biology of Peptides* (Meienhofer, J., Ed.) pp 45−49, Ann Arbor Science Publishers, Ann Arbor, MI.

43. Richarz, R., and Wüthrich, K. (1978) Carbon-13 NMR chemical shifts of the common amino acid residues measured in aqueous solutions of linear tetrapeptides H-Gly-Gly-X-L-Ala-OH, *Biopolymers 17*, 2133−2141.

44. Delepierre, M., Dobson, C. M., Karplus, M., Poulsen, F. M., States, D. J., and Wedin, R. E. (1987) Electrostatic effects and hydrogen exchange behaviour in proteins. The pH dependence of exchange rates in lysozyme, *J. Mol. Biol. 197*, 111−130.

45. Thurlkill, R. L., Grimsley, G. R., Scholtz, J. M., and Pace, C. N. (2006) pK values of the ionizable groups of proteins, *Protein Sci. 15*, 1214−1218.

46. Bai, Y., Milne, J. S., Mayne, L., and Englander, S. W. (1993) Primary structure effects on peptide group hydrogen exchange, *Proteins 17*, 75−86.

47. Linderstrøm-Lang, K. (1924) On the ionisation of proteins, *C. R. Lab. Carlsberg 15*, 1−29.

48. Better, M., Bernhard, S. L., Lei, S. P., Fishwild, D. M., and Carroll, S. F. (1992) Activity of recombinant mitogillin and mitogillin immunoconjugates, *J. Biol. Chem. 267*, 16712−16718.

49. Olmo, N., Turnay, J., González de Buitrago, G., López de Silanes, I., Gavilanes, J. G., and Lizarbe, M. A. (2001) Cytotoxic mechanism of the ribotoxin alpha-sarcin. Induction of cell death via apoptosis, *Eur. J. Biochem. 268*, 2113−2123.

50. Makarov, A. A., and Ilinskaya, O. N. (2003) Cytotoxic ribonucleases: molecular weapons and their targets, *FEBS Lett. 540*, 15−20.

51. Futami, J., Nukui, E., Maeda, T., Kosaka, M., Tada, H., Seno, M., and Yamada, H. (2002) Optimum modification for the highest cytotoxicity of cationized ribonuclease, *J. Biochem. (Tokyo) 132*, 223−228.

52. Pace, C. N., Laurents, D. V., and Thomson, J. A. (1990) pH dependence of the urea and guanidine hydrochloride denaturation of ribonuclease A and ribonuclease T1, *Biochemistry 29*, 2564−2572.

53. Font, J., Benito, A., Lange, R., Ribó, M., and Vilanova, M. (2006) The contribution of the residues from the main hydrophobic core of ribonuclease A to its pressure-folding transition state, *Protein Sci. 15*, 1000−1009.

54. Oliveberg, M., Vuilleumier, S., and Fersht, A. R. (1994) Thermodynamic study of the acid denaturation of barnase and its

55. Swint-Kruse, L., and Robertson, A. D. (1995) Hydrogen bonds and the pH dependence of ovomucoid third domain stability, *Biochemistry 34*, 4724−4732.

56. Tan, Y.-J., Oliveberg, M., Davis, B., and Fersht, A. R. (1995) Perturbed pKa values in the denatured states of proteins, *J. Mol. Biol. 254*, 980−992.

57. Laurents, D., Pérez-Cañadillas, J. M., Santoro, J., Rico, M., Schell, D., Pace, C. N., and Bruix, M. (2001) Solution structure and dynamics of ribonuclease Sa, *Proteins 44*, 200−211.

58. Trevino, S. R., Gokulan, K., Newsom, S., Thurlkill, R. L., Shaw, K. L., Mitkevich, V. A., Makarov, A. A., Sacchettini, J. C., Scholtz, J. M., and Pace, C. N. (2005) Asp79 makes a large, unfavorable contribution to the stability of RNase Sa, *J. Mol. Biol. 354*, 967−978.

59. Gasset, M., Mancheño, J. M., Lacadena, J., Martínez del Pozo, A., Oñaderra, M., and Gavilanes, J. G. (1995) Spectroscopic characterization of the alkylated alpha-sarcin cytotoxin: analysis of the structural requirements for the protein-lipid bilayer hydrophobic interaction, *Biochim. Biophys. Acta 1252*, 43−52.

60. García-Mayoral, F., García-Ortega, L., Álvarez-Garcia, E., Bruix, M., Gavilanes, J. G., and Martínez del Pozo, A. (2005) Modeling the highly specific ribotoxin recognition of ribosomes, *FEBS Lett. 579*, 6859−6864.

61. García-Mayoral, M. F., García-Ortega, L., Lillo, M. P., Santoro, J., Martínez del Pozo, A., Gavilanes, J. G., Rico, M., and Bruix, M. (2004) NMR structure of the noncytotoxic alpha-sarcin mutant Delta(7-22): the importance of the native conformation of peripheral loops for activity, *Protein Sci. 13*, 1000−1011.

62. Korennykh, A. V., Piccirilli, J. A., and Correll, C. C. (2006) The electrostatic character of the ribosomal surface enables extraordinarily rapid target location by ribotoxins, *Nat. Struct. Mol. Biol. 13*, 436−443.

63. Nozaki, Y., and Tanford, C. (1967) Proteins as random coils. II. Hydrogen ion titration curve of ribonuclease in 6 M guanidine hydrochloride, *J. Am. Chem. Soc. 89*, 742−749.

64. Elcock, A. (1999) Realistic modeling of the denatured states of proteins allows accurate calculations of the pH dependence of protein stability, *J. Mol. Biol. 294*, 1051−1062.

65. Forsyth, W. R., Antosiewicz, J. M., and Robertson, A. D. (2002) Empirical relationships between protein structure and carboxyl pKa values in proteins, *Proteins 48*, 388−403.

66. Alexov, E. (2004) Numerical calculations of the pH of maximal protein stability. The effect of the sequence composition and three-dimensional structure, *Eur. J. Biochem. 271*, 173−185.

67. Shaw, K. L., Grimsley, G. R., Yakovlev, G. I., Makarov, A. A., and Pace, C. N. (2001) The effect of net charge on the solubility, activity, and stability of ribonuclease Sa, *Protein Sci. 10*, 1206−1215.

68. Takano, K., Tsuchimori, K., Yamagata, Y., and Yutani, K. (2000) Contribution of salt bridges near the surface of a protein to the conformational stability, *Biochemistry 39*, 12375−12381.

69. Grimsley, G. R., Shaw, K. L., Fee, L. R., Alston, R. W., Huyghues-Despointes, B. M., Thurlkill, R. L., Scholtz, J. M., and Pace, C. N. (1999) Increasing protein stability by altering long-range coulombic interactions, *Protein Sci. 8*, 1843−1849.

70. Wunderlich, M., Martin, A., Staab, C. A., and Schmid, F. X. (2005) Evolutionary protein stabilization in comparison with computational design, *J. Mol. Biol. 351*, 1160−1168.

71. Perl, D., Mueller, U., Heinemann, U., and Schmid, F. X. (2000) Two exposed amino acid residues confer thermostability on a cold shock protein, *Nat. Struct. Biol. 7*, 380−383.

72. Loladze, V. V., Ibarra-Molero, B., Sanchez-Ruiz, J. M., and Makhatadze, G. I. (1999) Engineering a thermostable protein via optimization of charge-charge interactions on the protein surface, *Biochemistry 38*, 16419−16423.

73. Forsyth, W. R., and Robertson, A. D. (2000) Insensitivity of perturbed carboxyl pKa values in the ovomucoid third domain to charge replacement at a neighboring residue, *Biochemistry 39*, 8067-8072.

74. Santiveri, C. M., Santoro, J., Rico, M., and Jiménez, M. A. (2002) Thermodynamic analysis of beta-hairpin-forming peptides from the thermal dependence of 1H NMR chemical shifts, *J. Am. Chem. Soc. 124*, 14903−14909.

75. Endrizzi, J. A., Beernink, P. T., Alber, T., and Schachman, H. K. (2000) Binding of bisubstrate analog promotes large structural changes in the unregulated catalytic trimer of aspartate transcar-

bamoylase: implications for allosteric regulation, *Proc. Natl. Acad. Sci. U.S.A. 97*, 5077−5082.

76. Hammes-Schiffer, S. (2002) Impact of enzyme motion on activity, *Biochemistry 41*, 13335−13343.

77. Pace, C. N., Laurents, D. V., and Erickson, R. E. (1992) Urea denaturation of barnase: pH dependence and characterization of the unfolded state, *Biochemistry 31*, 2728−2734.

78. Spitzner, N., Lohr, F., Pfeiffer, S., Koumanov, A., Karshikoff, A., and Ruterjans, H. (2001) Ionization properties of titratable groups in ribonuclease T1. I. pK_a values in the native state determined by two-dimensional heteronuclear NMR spectroscopy, *Eur. Biophys. J. 30*, 186−197.

79. Laurents, D. V., Huyghues-Despointes, B. M., Bruix, M., Thurlkill, R. L., Schell, D., Newsom, S., Grimsley, G. R., Shaw, K. L., Trevino, S., Rico, M., Briggs, J. M., Antosiewicz, J. M., Scholtz, J. M., and Pace, C. N. (2003) Charge-charge interactions are key determinants of the pK values of ionizable groups in ribonuclease Sa (pI = 3.5) and a basic variant (pI = 10.2), *J. Mol. Biol. 325*, 1077−1092.

80. Zhou, H. X. (2004) Polymer models of protein stability, folding, and interactions, *Biochemistry 43*, 2141−2154.

81. Antosiewicz, J., McCammon, J. A., and Gilson, M. K. (1994) Prediction of pH-dependent properties of proteins, *J. Mol. Biol. 238*, 415−436.

BI061273V